Low Temperature Infrared Spectroscopy of Hydrogen in HKUST-1

Eric Rappeport

Physics and Astronomy
Oberlin College
April 1, 2016

Acknowledgments

I would like to thank my advisor Stephen Fitzgerald for his incredible help and patience with this project. He was always willing to take time and answer any and all of my questions. Through his guidance, I truly learned to enjoy and appreciate experimental physics. I am immensely grateful for this opportunity.

I want to thank the labmates who have helped so much with collection and analysis of the data presented here, as well as making the research such a fun experience. Thank you to Kinori Rosnow, Kai Shinbrough, and Josh Parker.

I would like to thank all of the physics and chemistry professors that taught me science over my four years at Oberlin. In particular I would like to thank professor Jason Stalnaker, who has taught me most of my physics knowledge. I also thank professor John Scofield for inspiring my love of physics, and professor Yumi Ijiri for helping me fall in love with materials and condensed matter physics. I also thank professor Rebecca Whelan for always being a supportive advisor and mentor. Lastly I would like to thank Jesse Rowsell, who was a tremendous role model who inspired me to work hard and showed me what a true passion for science looks like.

I would like to thank the other honors students, Peter Elgee and H. Perry Hatchfield, for being tremendously inspirational peers who have helped and supported me throughout the honors process. I additionally want to thank

all of my physics classmates and friends with whom I shared many classes and problem sets, as well as all of my friends who have made these past four years so much fun.

Lastly I would like to thank my parents and my brother for all the love and support they have given me.

Executive Summary

The purpose of this thesis is study the interactions between molecular hydrogen and the Metal Organic Framework HKUST-1. Because of the depletion of fossil fuels as well as the negative climate effects caused by their combustion, there has been extensive research into alternate fuel sources. One of the most promising candidates is hydrogen fuel, but its efficacy is limited by current hydrogen storage methods. Conventional techniques such as gas canisters are too heavy and dangerous to be used in lightweight vehicles, and so novel materials are needed. Metal Organic Frameworks, or MOFs, are highly porous compounds that could potentially solve this storage problem. At cryogenic temperatures, these materials can adsorb large quantities of hydrogen and could potentially be implemented as new storage devices. However no known MOF has yet been able to work effectively at sufficiently high temperatures for vehicle fuel cell operation. Current MOF research is thus focused on increasing our understanding of the hydrogen-MOF dynamics.In this thesis, we therefore implement infrared spectroscopy to study these interactions. By cooling the system to approximately 15 K, we are able to see distinctive peaks in the the spectrum of molecular hydrogen adsorbed to HKUST-1 that have not been observed previously. We therefore propose two possible mechanisms to explain the concentration dependence of these peaks. These results can be used to test new theories and eventually help steer MOF synthesis towards a practical solution to the hydrogen storage problem.

Contents

List of Figures

List of Tables

Glossary

Absorption: When a photon interacts with a material and induces a transition from one energy eigenstate to another.

Adsorption: The binding of a gas or liquid to the surface of a material, including the internal surface.

cm^{-1}: Wavenumbers, which are units of frequency. They are defined as $\frac{1}{\lambda}$ where λ is the wavelength of light in centimeters. They also can be used as units of energy via the relationship: $E = hc\frac{1}{\lambda}$.

Energy Conversions: 1 kJ/mol = 83.593 cm^{-1}. 1 cm^{-1} = 1.43 K.

J: The total orbital angular momentum quantum number. It effectively specifies the rotational energy eigenstate of the system.

Ortho Hydrogen: Molecular hydrogen in which the spin is in the S=1, or triplet, state, and the rotational quantum number J is odd.

Para Hydrogen: Molecular hydrogen in which the spin is in the S = 0, or singlet, state, and the rotational quantum number J is even.

Q Transitions: Transitions in which $\Delta\nu = 1$ and $\Delta J = 0$.

Redshift: The absolute value of the difference between the gas-phase frequency and the frequency in the bound state. This is called redshift because the frequency of the bound state is lower than that of the free molecule.

S Transitions: Transitions in which $\Delta\nu = 1$ and $\Delta J = 2$.

ν: The vibrational quantum number. It effectively specifies the vibrational energy eigenstate of the system.

Chapter 1

Introduction

Due to the severe climate effects associated with combustion of fossil fuel, there has been a tremendous interest in finding novel, renewable, and eco-friendly forms of energy [1]. A particularly promising option is hydrogen fuel. In fact the combustion of one gram of molecular hydrogen (H_2) with oxygen (O_2) releases nearly three times as much energy as one gram of gasoline, and the only byproduct is water [2]. The Department of Energy (DOE) furthermore predicts that the widespread use of hydrogen fuel cells in light-duty vehicles would cause a 55 to 90 % reduction in emissions when compared to todays gasoline vehicles [3]. Since fuels cells also directly convert chemical energy into electricity, they could achieve efficiencies of nearly 60 %, which is more than twice that of internal combustion engines [3]. However, several issues prevent the widespread use of hydrogen fuel, including a lack of effective storage methods. In order for molecular hydrogen to be a viable fuel source in automobiles, 5 to 13 kg of the gas would need to be consumed daily. The current procedure to store such large quantities of a gas is to either to liquefy it or compress it under excess pressure [2] and then store it in large canisters. Molecular hydrogen, however, liquefies at approximately 20 K, and so to store the gas as a liquid would require the vehicle to have

an expensive cryogenic system. Additionally, storing the gas in compressed form raises several safety concerns, for it would involve pressures as high as 200-300 bar [4]. Therefore new storage techniques are needed.

In order for hydrogen to be a viable option, the DOE has released several requirements for an ideal material. A storage system for a light-weight fuel cell vehicle needs to a have a weight capacity (kg H_2/kg) of 5.5 and a volumetric capacity of 40 g H_2/L [5]. Additionally the material must be able to operate at temperatures between -40 and 60 °C. To achieve these characteristics, the material must possess a binding energy such that large quantities of molecular hydrogen can be stored and extracted in an easy manner.

There are two ways of adsorbing a gas onto a material: chemisorption and physisorption. Chemisorption involves the formation of a chemical bond between the material and the adsorbent such that there is a significant charge transfer interaction between the two species as well as changes to the electronic structure [5]. Physisorption, on the other hand, is generally a much weaker process dominated by electrostatic and dispersion interactions. However, typical chemical bonds have very slow kinetics as well as desorption temperatures greater than 600 K, thereby limiting their applicability [4]. Physisorptive materials must therefore be used. The ideal adsorption enthalpy for such a material is predicted to be roughly 22 to 25 kJ mol^{-1} [6]. A variety of materials have been tested to meet these demands, including metal hydrides, chemical hydrides, inorganic nanotubes, organic materials, and clathrates [2]. A particularly promising candidate is a Metal Organic Framework (MOF). These compounds consist of metal ions bonded to organic ligands such that a large, highly porous compound is produced. In fact, MOFs possess internal surface areas regularly greater than 6000 m^2 per gram of material [7]. The ability to modify both the inorganic and organic subunits gives these compounds a tremendous amount of versatility, and as a result, they have found various uses in gas storage, catalysis, and biomedical

imaging [7].

However, no MOF yet proposed has been able to meet the Department of Energy goals, with most MOFs possessing an adsorption enthalpy between 5 and 12 kJ mol^{-1} [6]. A major reason for the inability to produce an ideal MOF lies in the complexity of predicting the material's behavior. MOFs have very large, complex unit cells, so first-principle, *ab initio* calculations are impossible. Furthermore, predicting dispersion interactions requires detailed knowledge of the wavefunctions. Traditional methods such as density functional theory (DFT) are notoriously bad at such time dependence [8], and their efficacy is thus limited in MOFs. Therefore current MOF research must focus on creating a firmer theoretical understanding of the binding processes in order to eventually reach the DOE requirements.

With this in mind, new experimental evidence must be presented in order to test the various theories. Infrared spectroscopy is a particularly powerful experimental tool for said tests. This technique operates by shining infrared radiation (IR) of various wavelengths at a sample of interest. Some of these frequencies will induce an excitation in the MOF and consequentially be absorbed by the sample, yielding a reduction in the measured intensity. This absorption can be plotted to yield a spectrum of peaks. Due to the complexity of these spectra, fitting them to a model is difficult, and so in principle, only the correct theory would be able to account for the observed patterns. This technique therefore acts as a tremendous test for examining the accuracy of proposed theories. However, IR peaks tend to broaden with increasing temperature, and MOFs possess low binding energies. It is therefore crucial to cryogenically cool the sample in order to gain the maximum useful information from an IR spectrum.

In order for the new theories to be tested accurately, the obtained spectra must be free of complications such as impurities or ambiguities in the crystal structure. It is therefore reasonable to employ IR onto a well-known, well-

studied MOF such as HKUST-1. This MOF has a known crystal structure, and neutron diffraction papers have confirmed the existence of 6 distinct binding sites [9][10]. Therefore, new IR information on this system could greatly help our understanding of gas-MOF interactions.

Chapter 2

Theory

The purpose of this chapter is to provide the necessary theoretical foundations to understand and analyze an infrared spectrum of molecular hydrogen in HKUST-1. With this in mind, the first section describes the theory behind infrared transitions, including the dipole approximation, transition probabilities, and the induced dipole mechanisms. The next section discusses the various motions of the molecular hydrogen in the MOF and the corresponding energy eigenstates. The third describes some important features of statistical mechanics, particularly the Boltzmann factor, and the fourth briefly explains the effect of symmetry requirements on molecular hydrogen. The final part provides some theory to explain the observed redshifts in the IR spectra.

2.1 Infrared Transitions

2.1.1 Multipole Expansion

According to classical electrostatics, any potential V from a charge density $\rho(\boldsymbol{r})$ can be expressed as a series of "poles":

$$V(\vec{r}) = \frac{1}{4\pi\epsilon_0}\sum_{n=0}^{\infty}\frac{1}{r^{n+1}}\int (r')^n P_n(\cos\alpha)\rho(\boldsymbol{r'})d\tau', \tag{2.1}$$

where $P_n(\cos\alpha)$ are the Legendre polynomials for the cosine of the angle between $\boldsymbol{r}$ and $\boldsymbol{r'}$ [11]. The potential expressed with the first 3 terms is:

$$\begin{aligned} V(\boldsymbol{r}) \approx & \frac{1}{4\pi\epsilon_0}\left[\frac{1}{r}\int \rho(\boldsymbol{r'})d\tau' + \frac{1}{r^2}\int r'\cos(\alpha)\rho(\boldsymbol{r'})d\tau'\right. \\ & \left. + \frac{1}{r^3}\int (r')^2(\frac{3}{2}\cos(\alpha)^2 - \frac{1}{2})\rho(\boldsymbol{r'})d\tau'\right] \\ & \approx \frac{1}{4\pi\epsilon_0}\frac{Q}{r} + \frac{1}{4\pi\epsilon_0}\frac{\sum \hat{r}_i p_i}{r^2} + \frac{1}{4\pi\epsilon_0}\frac{\sum\sum \hat{r}_i\hat{r}_j Q_{ij}}{r^3}, \end{aligned} \tag{2.2}$$

where Q is the total charge, or monopole, $\boldsymbol{p}$ is the dipole moment, and Q_{ij} is the quadrupole moment. Each sum in the above expression runs from 1 to 3 and corresponds to the 3 axes of the reference system. The quadrupole moment can be written in the general form:

$$Q_{ij} = \int (3r_i{}'r_j{}' - (r')^2\delta_{ij})\rho(\boldsymbol{r'})d\tau', \tag{2.3}$$

If the charge distribution consists of a series of point charges, then the dipole moment $\boldsymbol{p}$ is simply $\sum_{i=1} q_i x_i$, where i represents the ith particle. For molecular hydrogen and its isotopes, the monopole moment is zero. The dipole moment for H_2 and D_2 is also zero, but HD has a small dipole moment [12]. The quadrupole term for H_2 is zero in the J=0 state and nonzero in the J=1 state.

2.1.2 Transition Probabilities

The oscillating electric field of polarized light can be expressed classically as a traveling wave of the form: $e^{i(kx-\omega t)}$. For infrared radiation, the typical wavelengths of light are on the order of several thousand Å, whereas the

hydrogen molecule size is less than one Å. Therefore the electric field that the molecule interacts with can be considered spatially uniform (i.e. $E(x,t) = E_0 \cos(\omega t)$). The perturbation to the Hamiltonian is therefore:

$$H'(\boldsymbol{r},t) = \sum_{i=1} q_i E_0 x_i \cos(\omega t). \tag{2.4}$$

Using time-dependent perturbation theory [13], the probability of this perturbation inducing a transition from an energy level a to another energy level b is:

$$P_{a\to b} = \frac{|V_{ab}|^2}{\hbar^2} \frac{\sin^2[(\omega_0 - \omega)t/2]}{(\omega_0^2 - \omega^2)}, \tag{2.5}$$

where:

$$V_{ab} = \sum_{i=1} \langle \psi_b | q_i x_i | \psi_a \rangle, \tag{2.6}$$

where the term $\sum_{i=1} q_i x_i$ represents the dipole moment of the system. The probability of the photon inducing a transition is thus proportional to the integral V_{ab}. As can be seen, this integral term requires the dipole moment to change during the transition in order to be nonzero. Therefore ordinary molecular hydrogen, which possesses no dipole moment and does not acquire it through any excitation, is not infrared active. A dipole moment can however be induced via interactions with the MOF, allowing H_2 to be experimentally observed.

2.1.3 Induced Dipoles

There are two primary mechanisms to induce a dipole in the system: the polarizability and quadrupole mechanisms. As mentioned earlier, the J=0 state has no quadrupole moment, so the first mechanism is the only one applicable. The general characteristics of the two mechanisms are discussed below. For a more comprehensive overview of the polarizability of molecular hydrogen, please see Ref. [14].

Polarizability Mechanism

According to classical electrodynamics, the dipole moment μ of the hydrogen molecule induced by the electric field of the MOF is:

$$\boldsymbol{\mu} = \alpha \boldsymbol{E}, \tag{2.7}$$

where α is the polarizability of the molecule [11]. The polarizability is generally not uniform in all directions, and so a 3x3 matrix is needed in order to fully describe it. If one orientates the reference system such that the internuclear axis of molecular hydrogen is parallel to the z-axis, this tensor can be written in terms of $\alpha_{\parallel}$ and $\alpha_{\perp}$, which represents the components parallel and perpendicular to the z-axis respectively. These two values can be re-expressed into the more helpful form:

$$\begin{aligned} \bar{\alpha} &= \frac{1}{3}(\alpha_{\parallel} + 2\alpha_{\perp}), \\ \Delta\alpha &= \alpha_{\parallel} - \alpha_{\perp}, \end{aligned} \tag{2.8}$$

where $\bar{\alpha}$ represents the isotropic part of the polarizability, and $\Delta\alpha$ represents the anisotropic part [15]. In general the isotropic term is much larger than that of the anistropic, and so this mechanism activates only Q transitions in which $\Delta J = 0$ [16].

Quadrupole Mechanism

An alternative mechanism involves the electric field produced by the molecular hydrogen's quadrupole moment. This electric field will induce a dipole in the MOF, which in turn interacts with the photon to produce the absorption. Unlike with the previous mechanism, the polarizability of the MOF is not well known. However, the quadrupole moment possesses both isotropic

and anisotropic components, and this mechanism thus activates both the Q transitions as well as S transitions in which $\Delta J = 2$.

2.2 Modes of Motion

For the purposes of infrared radiation (IR), the energy levels of the hydrogenic electrons are too high to be excited, so we shall restrict our attention to the two protons. These molecules can perform three types of motion: they can translate, vibrate about the center of mass, and rotate. According to quantum mechanics, the wavefunction of the hydrogen molecule requires 6 coordinates: x,y,z for the first proton and x',y',z' for the second. However if the translations, vibrations, and rotations are not coupled, the wavefunction can be rewritten into the more intuitive form:

$$\psi(\boldsymbol{r_1}, \boldsymbol{r_2}) = \psi(x, y, z)\psi(\rho)\psi(\theta, \phi) = \psi_{trans}\psi_{vib}\psi_{rot}, \tag{2.9}$$

where x, y, z are the coordinates of the center of mass, ρ is the internuclear separation, and θ and ϕ are the normal spherical coordinates. These three types of motion are shown in Figure 2.1. We can therefore look at these separate modes of motion individually.

2.2.1 Vibrations

For a first approximation, it is useful to model the vibrations of the molecule as a simple harmonic oscillator. Solving the one-dimensional Schrödinger equation for this system yields the following formula for energies:

$$E_\nu = (\nu + \frac{1}{2})\hbar\omega, \tag{2.10}$$

where ν = 0,1,2,3,..., and $\omega = \sqrt{\frac{k}{\mu}}$, where μ is the reduced mass and k is the force constant. The separation between the two adjacent energy levels

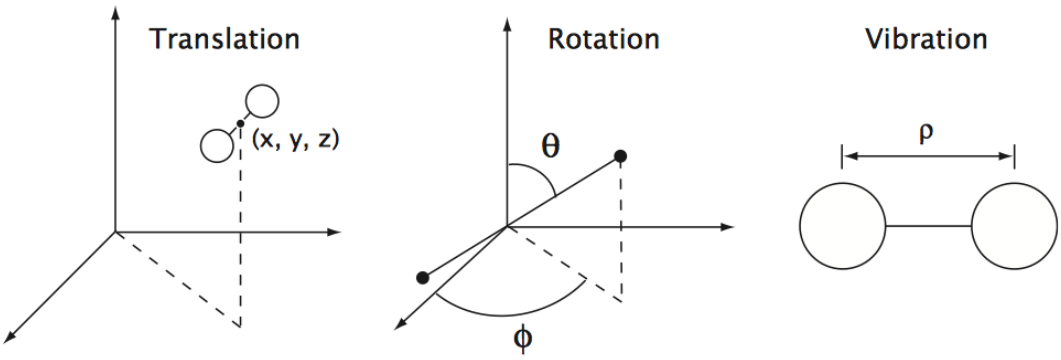

Figure 2.1: The 3 types of motions that a hydrogen molecule can undergo: translation, rotation, and vibration. Figure taken from Hugh Churchill's Thesis. [17]

is thus predicted to always be $\hbar\omega$. Additionally this model predicts that the transition frequencies for HD and D_2 scale as $\sqrt{\frac{3}{4}}$ and $\frac{1}{\sqrt{2}}$ respectively. Using the known transition frequency for hydrogen, 4161 cm^{-1}, the values predicted by the simple harmonic approximation for HD and D_2 are therefore 3604 cm^{-1} are 2942 cm^{-1}. The actual gas phase frequencies for HD and D_2 are found to be 3632 cm^{-1}, and 2994 cm^{-1} [18]. The discrepancies between the experimental and calculated values unsurprisingly suggest that the vibrational potential energy for the hydrogen molecule is not entirely harmonic, and anharmonic corrections are needed to more accurately model its behavior.

Anharmonic Potentials

While the simple harmonic oscillator serves as a solid first approximation, any true potential energy function needs to approach 0 as r approaches ∞. A more accurate approach would be to use the Morse potential:

$$U(r - r_e) = D_e(1 - e^{-\beta(r-r_e)})^2, \tag{2.11}$$

where D_e is the heat of dissociation (i.e. binding energy), β is a constant dependent on the anharmonicity, and r_e is the equilibrium distance [19]. The Schrödinger equation for this potential has been solved exactly, yielding the following formula for energies:

$$E_\nu = \hbar\omega_0(\nu + \frac{1}{2}) - \frac{\left|\hbar\omega_0(\nu + \frac{1}{2})\right|^2}{4D_e}, \tag{2.12}$$

where

$$\omega_0 = \beta\sqrt{\frac{2D_e}{\mu}}, \tag{2.13}$$

and μ is the reduced mass [20][15]. It can be seen that the first term in the energy expression closely resembles the simple harmonic oscillator energies with the second term acting as a correction. Because the second term grows with ν^2, the energy spacing between levels in this system decreases with increasing ν. This potential and its corresponding energy eigenvalues as well as those of the simple harmonic oscillator are shown in Figure 2.2.

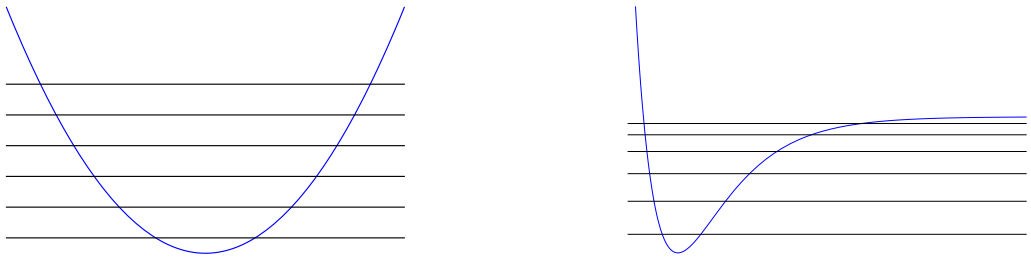

Figure 2.2: Simple Harmonic Oscillator Potential (left), and the Morse Potential (right). In both figures the blue curve represents the potential, and the black curves are the first 6 energy levels.

Selection Rules for Harmonic and Anharmonic Oscillators

For a 1-dimensional harmonic oscillator, the position operator x can be expressed as a linear combination of the ladder operators a_+ and a_-:

$$x = \sqrt{\frac{\hbar}{2\mu\omega}}(a_+ + a_-). \tag{2.14}$$

Therefore, the integral in the transition probability expression (equation 2.6) is:

$$\begin{aligned}\langle\psi_n|x|\psi_m\rangle =& \int \psi_n \sqrt{\frac{\hbar}{2\mu\omega}}(a_+ + a_-)\psi_m dx \\ =& \sqrt{\frac{\hbar}{2\mu\omega}}\left[\int \psi_n(\sqrt{(m+1)\hbar\omega})\psi_{m+1}dx + \int \psi_n(\sqrt{(m)\hbar\omega})\psi_{m-1}dx\right] \\ =& \sqrt{\frac{\hbar}{2\mu\omega}}\left[\sqrt{(m+1)\hbar\omega}\delta_{n,m+1} + \sqrt{(m)\hbar\omega}\delta_{n,m-1}\right],\end{aligned} \tag{2.15}$$

where the two δ terms are Kronecker deltas [13]. Thus the harmonic potential predicts that the only transitions possible are ones in which $\Delta\nu = \pm 1$. Any observed overtone transitions (i.e $\Delta\nu = 2$) therefore arise from the anharmonicity of the potential. These overtone peaks should correspondingly be much weaker than those of the fundamental.

2.2.2 Rotations

Rigid Rotator

The simplest model of rotation is that of a rigid rotator in which two masses rotate freely at a fixed distance about an axis. Using the equivalent quantum-mechanical term for rotational kinetic energy, the time-independent Schrödinger equation becomes:

$$\frac{\hat{L}^2}{2I}\psi = E\psi, \tag{2.16}$$

where $\hat{L}^2$ is the square of the total angular momentum operator, and I is the moment of inertia. We know that the eigenstates for this operator are the spherical harmonics with a corresponding eigenvalue of $\hbar^2 J(J+1)$ [13], where $\hbar$ is the reduced Planck's constant. Therefore, the energy eigenvalues for the rigid rotor are:

$$E_J = \frac{\hbar^2 J(J+1)}{2I} = B_\nu J(J+1), \tag{2.17}$$

where B_ν is the rotational constant dependent on the quantum number ν. In wavenumbers this constant has the value $\frac{h}{8\pi^2 cI}$ [19], where h is Planck's constant, I is the moment of inertia, and c is the speed of light. For molecular hydrogen, $B_0 = 59.3\ \text{cm}^{-1}$ and $B_1 = 56.4\ \text{cm}^{-1}$ [21]. Additionally, the energy difference between the J=0 and J=1 states is 14.7 meV.

2.2.3 Translations

To fully model the translational motion of molecular hydrogen in a MOF, one would need to know the potential energy surface generated by the framework. As mentioned in the introduction, the complexity of these materials means that this task is very difficult. We therefore can only provide a rough approximation to this potential by treating it as an isotropic, 3-dimensional simple harmonic oscillator. The energy formula for this oscillator is:

$$E_\nu = \hbar\omega(\nu + \frac{3}{2}), \tag{2.18}$$

where ν is the normal vibrational quantum number. Note that since this potential is 3-dimensional, there exist degenerate energy eigenstates. For HKUST-1, Inelastic Neutron Scattering data [10] suggests that the energy separation between the translational ground state and first excited state is roughly 80-94 cm^{-1}.

2.3 Boltzmann Statistics

In statistical mechanics, it is common to classify space into the system of interest and a thermal reservoir. With this distinction, the total multiplicity of a particular configuration can be written as:

$$\Omega_{Total} = \Omega_R \Omega_S, \tag{2.19}$$

where Ω is the total number of microstates, and the subscripts R and S stand for the reservoir and system respectively. The total number of states in which the system is in a particular microstate is therefore the multiplicity of the reservoir. Note that this number is a function of energy, $\Omega(U-E)$, where U is the total energy and E is the energy in the system. The entropy S of this particular microstate is thus:

$$S = k_b ln(\Omega_R(U-E)), \tag{2.20}$$

where k_b is Boltzmann's constant. Now if we assume that the reservoir is much larger than the system such that E << U, the above expression can be Taylor expanded about U. This yields:

$$\begin{aligned} S(U-E) &= k_b ln(\Omega_R(U)) + (\frac{\partial S}{\partial U})_V|(-E) \\ k_b ln(\Omega_R(U-E) &= k_b ln(\Omega_R(U)) - E/T, \end{aligned} \tag{2.21}$$

where we have used the entropy-derived definition of temperature. Therefore the total number of states for this particular system microstate is:

$$\Omega_R(U-E) = \Omega_R(U) e^{\frac{-E}{k_b T}}. \tag{2.22}$$

The probability of the system being in a state with energy E is thus proportional to:

$$P(E) \propto e^{\frac{-E}{k_b T}}. \tag{2.23}$$

The above proportionality factor is known as the Boltzmann factor. To get the actual probabilities, one notes that the sum of the Boltzmann factors over all the microstates must be 1. Therefore the individual probability of an energy state being occupied must be:

$$P(E) = \frac{D_i e^{\frac{-E}{k_b T}}}{\sum_i e^{\frac{-E_i}{k_b T}}}, \tag{2.24}$$

where D_i is the degeneracy of that energy state. The term in the denominator is known as the partition function. The above probabilities are most useful when the temperature of the system is fixed, and so for our purposes, the probability of occupying a particular energy state at thermal equilibrium is given by the above equation.

2.4 Forms of Hydrogen

Since the two protons of the hydrogen molecule are indistinguishable, spin-1/2 fermions, the total wavefunction that describes them must be antisymmetric under exchange of the particles. This total wavefunction can be written as the product of the spatial wavefunction multiplied by a spinor χ:

$$\psi_{tot} = \psi_{trans}\psi_{vib}\psi_{rot}\chi. \tag{2.25}$$

Since this molecule involves the addition of two spin-1/2 particles, the total spin of the system S can be either 0 or 1. The spin-0 state is nondegenerate, and is thus known as the singlet state, whereas the $S = 1$ state is triply degenerate, and is thus the triplet state. A more common name for this two states is Para and Ortho Hydrogen respectively. Additionally the singlet state is antisymmetric under exchange and the triplet is symmetric. Therefore if the hydrogen molecule is in the singlet state, the spatial wavefunction must be symmetric. This is only possible if the rotational quantum number

J is even, for the vibrational and translational wavefunctions depend only on the internuclear separation and center of mass respectively. Conversely, if the molecule is in the triplet state, J must be odd. Molecular hydrogen can therefore be "trapped" in the J=1 state even as temperatures approach 0, so long as the spin state does not change. On the other hand, molecular deuterium consists of the addition of two bosons, and so the total wavefunction must be symmetric. The J=0 state is thus no longer associated with $S = 0$, but rather with $S = 1$. This symmetrization requirement also means that transitions where $\Delta J = \pm 1$ are not possible. Consequently, the rotational quantum number J can only change by 0 or 2 during an absorption.

2.5 Redshifts

It is quite common in MOFs to see the Q and S peaks of molecular hydrogen to be at significantly lower frequencies than their gas-phase values. A first approximation to explain this redshift is to say that the interaction energy is linearly dependent on the isotropic polarizability of molecular hydrogen. The first excited vibrational state (i.e. $\nu = 1$) possesses a polarizability roughly 1.1 times greater than that of the ground state [14]. Therefore the decrease in the energy of the first excited state is suspected to be 10 % larger than that of the ground state. The energy difference between the two states is therefore reduced by roughly 1/10 of the interaction energy. This reduction is the observed redshift. While this only serves as a first approximation, it has been shown to work reasonably for most MOFs (see Figure 3.5).

Chapter 3

HKUST-1

3.1 General Structure

The empirical formula for activated HKUST-1 is $Cu_3(BTC)_2$, where BTC = benzene-1,3,5-tricarboxlyate. Typically during synthesis solvent molecules are bonded onto the copper atoms, and so the material must be heated in order to remove these molecules and create the desired open metal sites. HKUST-1 forms a face-centered (fcc) cubic crystal with large, square-shaped pores roughly 9 by 9 Å in size [22]. The primary structural unit is a copper dimer bonded to four carboxylates such that each carboxylate is connected to both coppers. This arrangement is known as a copper paddlewheel, and we will refer to it as such from this point forward. These dimers then act as the vertices for a large octahedral unit, and these units are subsequently the vertices of the largest pore. In addition to the major cubic pore, each octahedral unit also contains a large pore through which hydrogen can permeate. The unit cell is thus large and contains 156 atoms [23]. Depictions of this structure along two different crystallographic axes are shown below in Figure 3.1.

A close-up of one of the copper paddlewheels is shown in Figure 3.2.

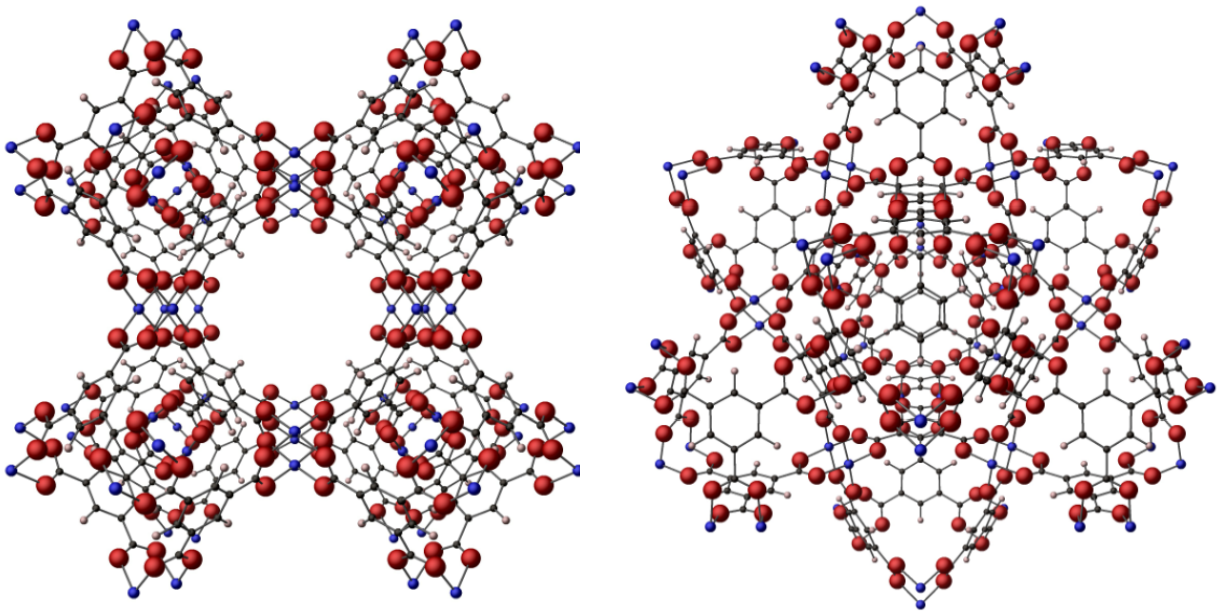

Figure 3.1: The HKUST-1 Unit Cell viewed along {100} (left)and {111} (right) planes.The black atoms are carbon, the red are oxygen, the beige are hydrogen, and the blue are copper.

3.2 Binding Sites

Several neutron diffraction studies have been performed on HKUST-1 ([9],[10]). These studies demonstrated that the primary binding site is the coordinatively unsaturated copper atom, with the molecular hydrogen lying at an approximate distance of 2.4 Åfrom the copper. This number however changes slightly with the amount of molecular hydrogen added, achieving a value of 2.49 Å at 2 H_2/Cu, while shrinking to 2.35 Å at 6 H_2/Cu added. The second adsorption site is in the"window" of the octahedral pores [10], as seen in Figure 3.3.

The third site sits within the octahedral pore, as shown in Figure 3.4. The other binding sites begin to be populated at greater concentrations, and since the focus of this thesis is on the low concentration effects, they are not shown

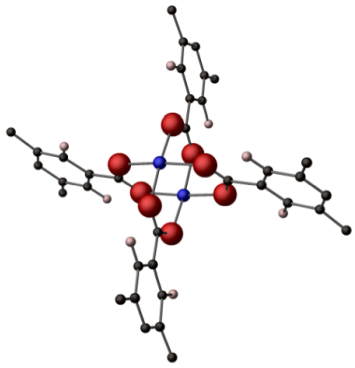

Figure 3.2: A Close-up of the Copper Paddlewheels of HKUST-1. The black atoms are carbon, the red are oxygen, the beige are hydrogen, and the blue are copper.

here. Additionally, the order of these binding sites is dubious, for as we will show in section 5.3, the anneal temperatures used in the studies (30-50 K for Peterson et al. and 35 K for Callear et al.) were too low to achieve thermal equilibrium, thereby calling into question the validity of those binding orders.

3.3 Binding Energies

The binding energy for HKUST-1 found by several different groups is shown in Table 5.1.

This binding energy, as well as the redshift of the Q peaks, is compared to those in other MOFs in Figure 3.5, as well as the redshift from the gas-phase molecular hydrogen frequency to the lower one seen in the MOF. Note that the plotted binding energy for HKUST-1 is the value found by Rowsell *et al.* From this graph it can be easily seen that there exists a correlation between the binding energy and the redshift. If we approximate this correlation to be linear, then the expected redshift per binding energy (in cm^{-1}) is approximately 0.1, thereby agreeing with the polarizability argument mentioned

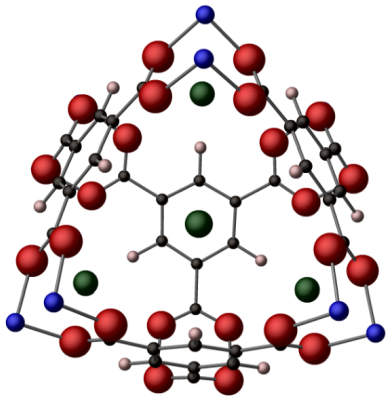

Figure 3.3: The 2nd adsorption site in HKUST-1. The green atoms here represent the molecular hydrogen. This site is one of the openings to the octahedral pore. Note that this figure is a cross-section of the pore.

earlier in section 2.5.

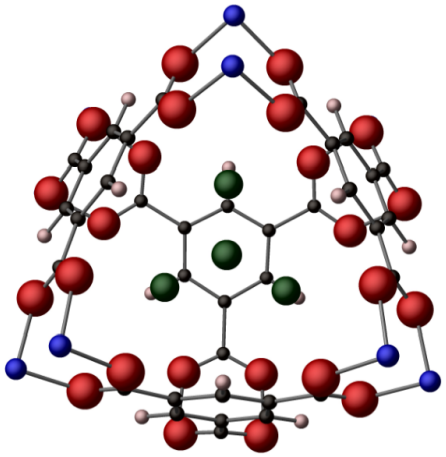

Figure 3.4: The 3rd adsorption site in HKUST-1. The green atoms here represent the molecular hydrogen. This site is one of the openings to the octahedral pore. Note that this figure is a cross-section of the pore.

Table 3.1: Measured binding energies for HKUST-1.

Binding Energy (kJ/mol)	Researchers
6.8	Rowsell [24]
10.1	Vitillo et al. [25]
6-10	Liu [26]
10.1 ±0.7	Bordiga et al. [27]

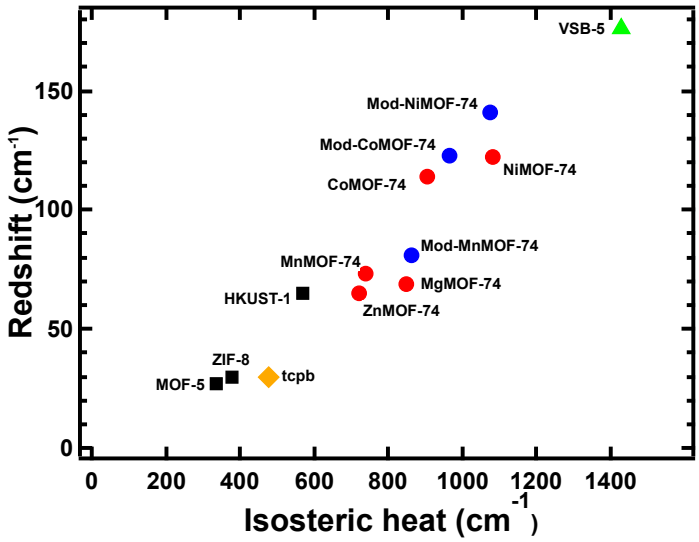

Figure 3.5: Redshift vs Isoteric Heat (Binding Energy) for Various MOFs. Note that there appears to be a roughly linear correlation between the redshift and the binding energy.

Chapter 4

Experimental Procedure

4.1 Introduction

Infrared spectroscopy operates by shining a polychromatic source of infrared radiation at a sample and observing the decrease in intensity at certain wavelengths. By referencing this intensity against a background spectrum, one generates an absorption spectrum. These absorptions, however, can only be observed if the radiation induces a change in the dipole moment of the molecule. Thus free molecular hydrogen is infrared inactive and is not observed. As a result, any hydrogen peaks arise from a dipole induced by interactions between the MOF and the molecular hydrogen. These interactions are typically weak, and so the effective path length needs to be large in order to observe them [15]. However, the longer path increases scattering off of the crystal grains, thereby reducing the signal.This leads to a paradox where a longer path is necessary to observe the hydrogen-MOF peaks, but at the same time reduces the signal, making peaks harder to discern. The solution to this problem is Diffuse Reflectance Infrared Fourier Transform Spectroscopy (DRIFTS).

4.2 Interferometry

The relative intensities of the light frequencies are found using interferometry. DRIFTS uses a beam splitter to cut the source light into two smaller beams. One beam is sent to a stationary mirror whereas the other travels towards a movable mirror. Both recombine at the detector, where an interference pattern is observed. When there is zero path difference between the two beams, constructive interference occurs. However, if the path difference is $\frac{\lambda}{2}$, then destructive interference results. By changing the position of the movable mirror at a constant rate, this pattern becomes a function of time. The above equation, however, only describes the interference of a single wavelength. With a polychromatic source, the detected wave is the superposition of the interference of all wavelengths. The signal is thus Fourier transformed.

4.3 Diffuse Reflectance Infrared Fourier Transform Spectroscopy

The source beam enters the chamber via a CaF_2 window. Two plane mirrors direct the light towards an ellipsoidal mirror that focuses it into the sample chamber via a sapphire window. The radiation then scatters off multiple grains, eventually exiting the chamber via another sapphire window, where another set of mirrors refocuses the light and sends it to the detector. This scattering increases the path length, thereby allowing absorptions to be observed. Using this technique, only milligram amounts of the sample are needed. A schematic is shown in 4.1.

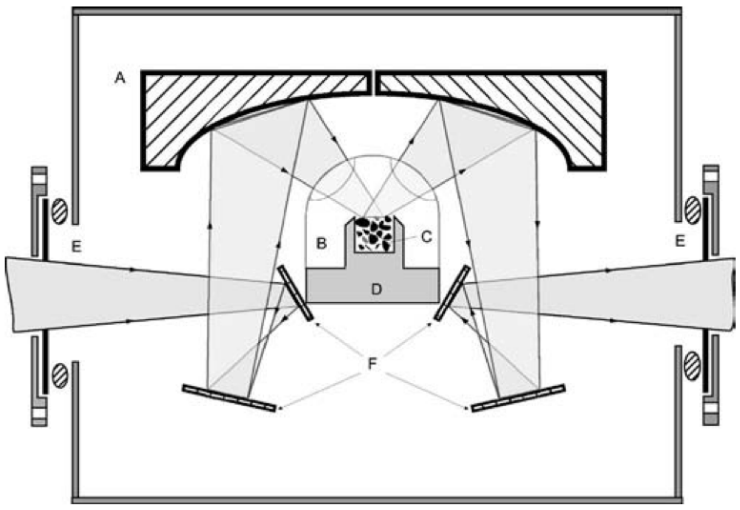

Figure 4.1: Schematic of the DRIFTS Optics.The radiation enters the box via a CaF_2 window (E), where two plane mirrors and an ellipsoidal mirror (A and F) focus it into the sample chamber (B). The light hits the sample (C), which is placed in a copper holder (D), where it scatters of multiple grains before exiting through a second CaF_2 window. Image taken from Ref. [28].

4.4 Cryogenics

The DRIFTS optics successfully detects IR adsorption. However, the molecular hydrogen-MOF interaction is sufficiently weak that at room temperature, little to no molecular hydrogen is bound to the MOF. The system must therefore be cooled to cryogenic temperatures for these interactions to be observed. Additionally, IR peaks increase in sharpness and depth as the temperature decreases, yielding more informative spectra with a smaller degree of convolution.

This cooling is achieved via a custom built vacuum chamber. A liquid-helium Janis Research Company closed-cycle ST-300T cryostat with a cold finger is attached to a copper sample mount. In order to use the rather large

DRIFTS optics, this mount rests inside a 15 x 12 x 15 cm^3 aluminum box [28]. The lower portion of the cryostat vacuum wall is removed, and the entire box acts as the new vacuum chamber. A turbomolecular pump is used to create the vacuum. As mentioned above, radiation enters and exits the chamber via two CaF_2 windows, where mirrors focus and reflect the beam towards the sample mount. This mount consists a copper sample holder screwed into a copper slab that is soldered onto the sample mount. A dome with two flat sapphire windows is placed over this holder and sealed with indium. The metal seal is necessary, for standard O-rings fail at these low temperatures. A schematic of the complete system is shown in Figure 4.2.

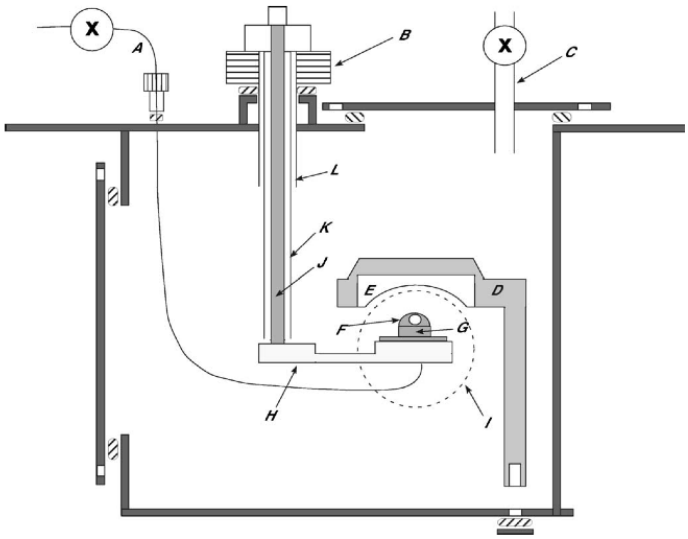

Figure 4.2: A schematic of the complete, cryogenic system used for DRIFTS. (A) gas-line, (B)manual height adjuster, (C) evacuation line, (D) DRIFTS Optics Mount, (E) ellipsoidal mirror, (F) high-pressure dome, (G) sample holder, (H) copper slab, (I) CaF_2 window, (J) cold finger,(K) radiation shield,(L) cryostat vacuum wall. Image taken from ref. [28].

4.5 Sources, Detectors, and Filters

Both a quartz-halogen and globar source were used in the course of the experiment. The main detection method was a Mercury Cadmium Telluride (MCT) detector in conjunction with a broad filter that minimizes the amount of visible light that reaches and potentially heats the sample. A consequence of this filter is that the frequencies below 3500 cm^{-1} cannot be discerned. The other detector used consisted of Indium Gallium Arsenide (InGaAs). This detector is roughly a hundred times more sensitive than the MCT detector [29], meaning that it easily saturates. A narrow bandpass filter was therefore used with this detector.

4.6 Data Acquisition

The amount of gas adsorbed was measured by monitoring the pressure difference. The gas is initially loaded into this volume at a desired pressure, before being sent to the sample. When it is sent, the total volume occupied by the gas consists of the calibrated volume, the gas line, and the sample dome. Since the volumes of all three of these are known, as well as the temperature, the difference between the original and the new pressure can be used to calculate the amount of molecular hydrogen adsorbed by the MOF. We additionally measure the mass of the MOF before it is loaded into the sample holder, thereby allowing calculations of intensive quantities such as amount of gas adsorbed per mol of sample.

Absorbance spectra were created by referencing the spectra of HKUST-1 with molecular hydrogen to a spectrum without it. The absorbance A is defined to be:

$$A = -log\frac{I}{I_0}, \tag{4.1}$$

where I is the intensity of the spectra with molecular hydrogen, and I_0 is the

intensity of the pure, solely-MOF spectra. Most spectra shown here are the average of 100 scans at 0.25 cm^{-1} resolution. To calculate the areas of these absorbance peaks, the peaks were fit to either Lorentzian peaks, Gaussian peaks, or a combination of both (see Figure 8.3 in Appendix). These areas should be proportional to the number of hydrogen molecules.

4.7 HKUST-1 Synthesis

The HKUST-1 used in these experiments was synthesized by the Stavila research group at Sandia National labs. These powders were formed from a solution of $Cu(NO_3)_2 \cdot 2.5\ H_2O$ and H_3BTC in equal volumes of ethanol (EtOH), DMF, and H_2O. This solution was then heated to 85 °C for 20 hours. The solid product was then filtrated and washed with DMF to remove the unreacted reagents. The powder was immersed in DMF for 2 hours, and the supernatant was decanted. The immersion and decanting was repeated eight times, followed by eight washings with $CHCl_3$. These crystals were then heated to 185 °C under vacuum for 16 hours to yield the solvent-free, activated HKUST-1.

4.8 Procedure

The sample was stored in an argon glove box under excess pressure. The copper sample holder, dome, and sample mount were brought inside the box, and the sample was loaded onto the cup and screwed to the mount. The dome was then placed on top and sealed inside the glove box to prevent exposure to air. The entire apparatus was placed into the vacuum chamber.

Before loading the desired gas, a small dose of helium is added first. This gas should not bind to the MOF, and so it can act as exchange gas to ensure thermal equilibrium. The desired gas was loaded into the sample at base

temperature (15 K), followed by an anneal. This anneal consists of rapid heating to a set temperature followed by cooling down at a rate of 5 K/min. An anneal temperature of 75 K was found to be optimal.

Chapter 5

Results

To understand hydrogen binding in HKUST-1, we took many spectra of H_2, D_2, and HD in the MOF in both the fundamental and overtone regions. The observed frequencies of these various peaks as well as the values for the free, gas-phase molecules are shown in Table 5.1. Note that the we were unable to observe the fundamental deuterium peaks.

5.1 The Q region for hydrogen in HKUST-1

Spectra of HKUST-1 with and without molecular hydrogen at 15 K are shown in Figure 5.1 for 0.45 H_2/Cu added. The most striking difference between the two are the very sharp, deep peaks near 4,100 cm^{-1} that are roughly 60 cm^{-1} below the gas phase $Q_1(1)$ and $Q_1(0)$ frequencies. In this notation, the subscript number refers to the vibrational quantum number of the excited state. The initial vibrational state is always the ground state. The (1) refers to the ortho hydrogen and (0) refers to the para hydrogen. To gain physical significance, the spectra are converted into absorbances (see section 4.6). In principle, as long as an absorption occurs at the same frequency and intensity, it should not appear in the new spectra. Therefore, much of the MOFs

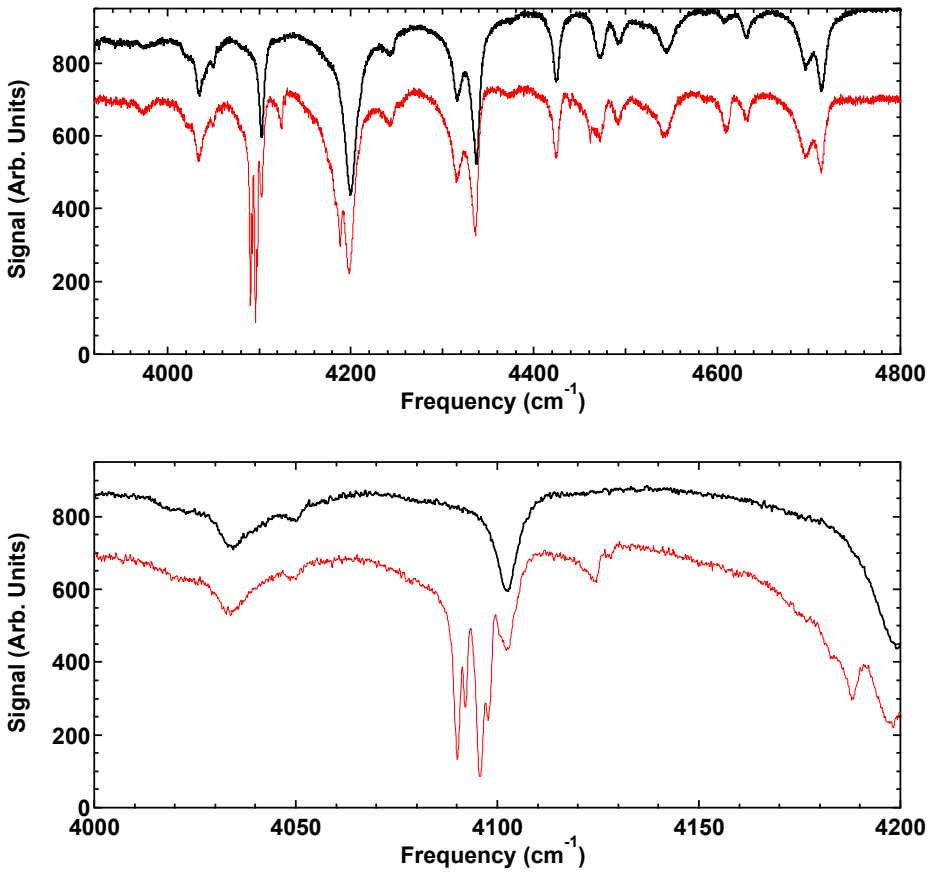

Figure 5.1: Typical transmittance spectra of HKUST-1 with (red) and without (black) H_2 added. The upper spectra show both the Q and S regions, whereas the lower ones focus on the Q region. The spectra were collected at approximately 15 K at 0.25 cm^{-1} resolution. Note that the pure MOF spectrum is offset for clarity.

Table 5.1: Table of the observed adsorption frequencies of H_2, D_2, and HD in both the free and HKUST-1 bounded forms.

	$Q_1(0)$	$Q_1(1)$	$Q_2(0)$	$Q_2(1)$
H_2 Free	4161.2[a]	4155.2[a]	8087[b]	8075.3[c]
H_2 in HKUST-1	4095.9	4090.2	7953	7942.5
	4097.9	4092.1		
D_2 Free	2993.5[a]	2991.4[a]	5868.5[b]	5863.9[e]
D_2			5765	
HD Free	3632.1[a]	3628.2[a]	7087[f]	7079.2[d]
HD in HKUST-1	3573		6966	
			6969	

a) Ref [30]

b) Ref [31]

c) Ref [32]

d) Ref [33]

e) Ref [34]

f) Calculated from Ref [34]

peak result in zero absorption, leaving a cleaner, easier to read spectrum. However, run to run variation as well as modification of the MOF due to the hydrogen may prevent full cancellations. Further identification of these sharp peaks can be confirmed using statistical mechanical arguments. Since the number of molecular hydrogen in a particular energy configuration is proportional to $e^{\frac{-E}{k_b T}}$, the energetic preference for the primary site relative to that of the secondary sites becomes greatly enhanced at lower temperatures. Both Peterson et al. [9] and Callear et al. [10] have noted that at temperatures of 3.5 and 10 K respectively, this primary site is the coordinatively unsaturated copper atom. Thus at our base temperature of 15 K, we assume that all of the hydrogen molecules should bind directly to this primary site so long as it remains available. We can therefore confidently assign these peaks to be the those of the molecular hydrogen physisorbed onto the copper paddlewheels.

There are several other noticeable differences between the spectra with and without molecular hydrogen. At roughly 4130 cm^{-1}, there is a small peak, which we believe to arise from molecular hydrogen bound to the secondary sites of HKUST-1 (See Figure 8.1 in the appendix). The deep peak at 4180 cm^{-1} is likely the Q_1 transitions coupled with a translation [15]. Finally the small peak near 4440 cm^{-1} is likely an S peak [15].

Absorbance spectra for concentrations of 0.1 (blue), 0.22 (red), 0.45 (orange), 0.7 (green), 0.9 (purple), and 1.37 (black) H_2/Cu are shown in Figure 5.2. There are two initial peaks at 4090 cm^{-1} and 4096 cm^{-1}. These mostly agree with the observed IR features found by Bordiga et. al (ref.[27]), and that group identified these peaks as belonging to the $Q_1(0)$ and $Q_1(1)$ transitions respectively. Further confirmation of this assignment can be made by noting that the separation of the two initial peaks is roughly 6 cm^{-1} (see Table 5.1) [18], as well as the fact that the higher wavenumber peak is seen to grow in time as the first diminishes, thereby suggesting ortho to para-hydrogen

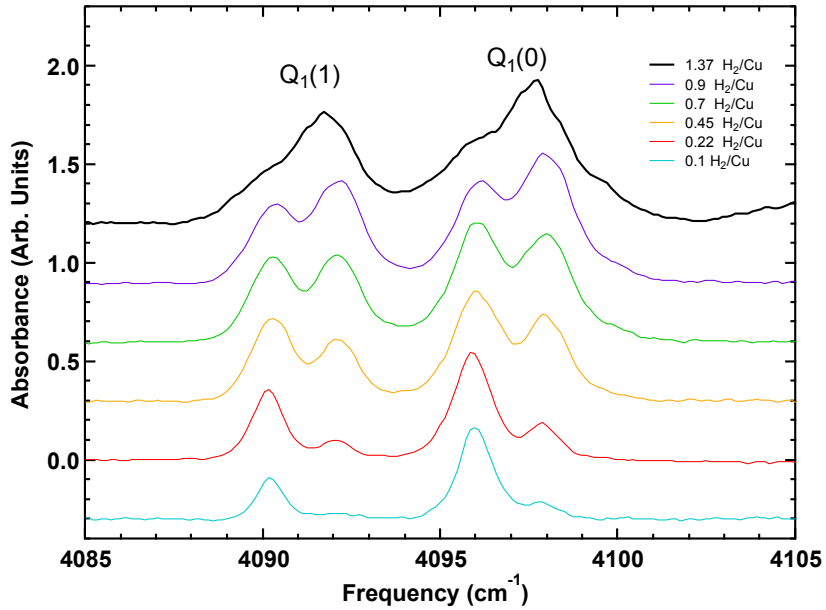

Figure 5.2: An absoprtion spectrum for the $Q_1(0)$ and $Q_1(1)$ transitions in HKUST-1. Note that the two peaks at lower wavenumbers correpsond to the $Q_1(1)$ and the higher correspond to $Q_1(0)$. The spectra are offset for clarity.

conversion. As the concentration is increased, two new peaks are observed at 4092 and 4098 cm^{-1}. Upon the addition of more hydrogen, the original peaks reach a maximum intensity before decreasing, whereas the newer peaks grow and broaden. These trends suggest that the two sets of peaks are not independent. Therefore if these correspond to molecular hydrogen bound to the primary site, there is evidence for either direct hydrogen-hydrogen interactions or hydrogen-hydrogen interactions mediated by the MOF.

A preliminary interpretation of these phenomena would be to assume hydrogen-hydrogen interactions across the copper paddlewheel. As FitzGerald et al. showed for MOF-5 [35], the production of side-bands around the $Q_1(1)$ and the absence of said side-bands around $Q_1(0)$ suggested the influence of Electric Quadrupole-Quadrupole interactions, which only exists in the J=1 state (i.e. the J=0 state is very nearly spherical and does not possess a quadrupole moment). In contrast, the $Q_1(0)$ and $Q_1(0)$ peaks for HKUST-1 have virtually the same sideband behavior, suggesting that the primary hydrogen-hydrogen interaction does not involve the quadrupole moment. This interaction must therefore be independent of the hydrogen molecule's orientation [36]. One can make an initial prediction of this interaction by approximating the hydrogen to be the same as those in solid molecular hydrogen. Since the smallest possible distance between two hydrogen molecules is 5.6 Å, the solid molecular hydrogen model predicts an interaction energy less than 10 K ([36], [37]). With such a low interaction energy, this effect could not be responsible for the observed 2 cm^{-1} splitting. The hydrogen must therefore be significantly perturbed from its molecular solid state.

5.2 The HD Overtone Spectrum

Despite the apparent trends shown in the fundamental H_2 spectra, several issues complicate further analysis. First is ortho to para conversion. As mentioned in section 2.4, the relaxation from the J = 1 to the J=0 is forbidden in the absence of a magnetic field, and so in principle, the 3:1 room temperature ortho-to-para ratio should be maintained as the system is cooled. This is not the case, however, and we observed that conversion between the two rotational states can occur in a few hours, thereby changing over a single-data collecting period. This is most likely a result of the magnetic nature of the Cu ions [38]. Furthermore these conversions do not appear to maintain the absorption peak areas, thereby hindering their use as measurements of the relative concentrations of molecules. An additional complication is the small separation (2 cm^{-1}) between the peaks. This leads to significant convolution of the peaks, which in turn increases the uncertainty in accurately fitting them to either a Lorentzian or Gaussian.

A way to overcome these obstacles is to study HD in the overtone region. Since HD is not a symmetric molecule, relaxation between the J=1 and J=0 states is not forbidden. Thus as the system reaches thermal equilibrium, the relative concentrations of molecules in the J=0 to the J=1 state should be constant with time. Furthermore, since an overtone transition is expected to be roughly twice that of the fundamental [39], any inherent energy difference between states will be exaggerated, increasing the separation of the IR peaks. This leads to an overall reduction in peak convolution, yielding more accurate fits.

The observed HD overtone peaks at various concentrations are shown in Figure 5.3. The spectra are offset for clarity, with higher concentrations appearing higher on the graph. The two vertical lines represent the central frequency of the peaks at low concentrations. As can be seen, the initial

spectrum contains one distinct peak at 6966 cm^{-1}. With increasing concentration, this peak shifts to higher frequencies and grows larger, achieving a maximum area at a concentration of 0.8 to 0.9 HD/Cu. After this the intensity of the peak diminishes. An additional second peak at 6969 cm^{-1} appears first at a concentration of 0.22 HD/Cu, and monotonically increases in magnitude with higher concentrations. This peak further undergoes a redshift at a concentration of 1.11 HD/Cu. Therefore between the minimum and maximum concentrations, the HD spectrum exhibits 2 peaks that are separated by roughly 3 cm^{-1}. This splitting corresponds directly to the 2 cm^{-1} separation observed in the Q region. This relationship can be rationalized by assuming that interactions with the MOF are nearly identical between H_2 and HD, meaning that the size of the splitting relative to the free, gas-frequency should be constant [39]. Thus using the splitting found for the molecular hydrogen, the splitting in the HD overtone is expected to be a little larger than 3 cm^{-1}. These peaks additionally exhibit similar concentration dependencies as those in H_2, thereby strengthening their association. There is a small but noticeable third bump at higher concentrations centered at 6963 cm^{-1}. Temperature-dependency studies (see section 5.3) confirmed that this feature is the J=1 overtone.

5.3 Thermal Equilibrium

In order to accurately model the energetics of the various molecular hydrogen interactions with a particular metal organic framework, it is crucial that the hydrogen is in thermal equilibrium with stable concentrations of both the free and bound form. At cryogenic temperatures, the molecules have so little thermal energy that they essentially bind to the nearest available site, even if a lower energy state is possible. Additionally, the molecular hydrogen must enter the MOF grains from the outside, meaning that the exterior surface

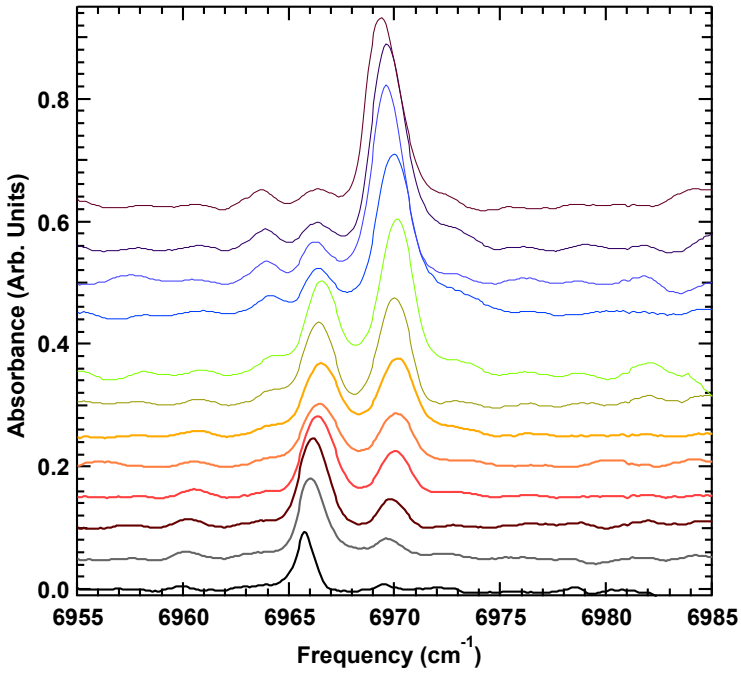

Figure 5.3: Adsoprtion spectra for the HD overtone transitions in HKUST-1 at 0.11 (black), 0.22 (gray), 0.33 (brown), 0.44 (red), 0.55 (dark orange), 0.66 (orange), 0.77 (dark green), 0.88 (light green), 1.11 (blue), 1.22 (purple), 1.33 (violet), and 1.44 (magenta) HD/Cu.

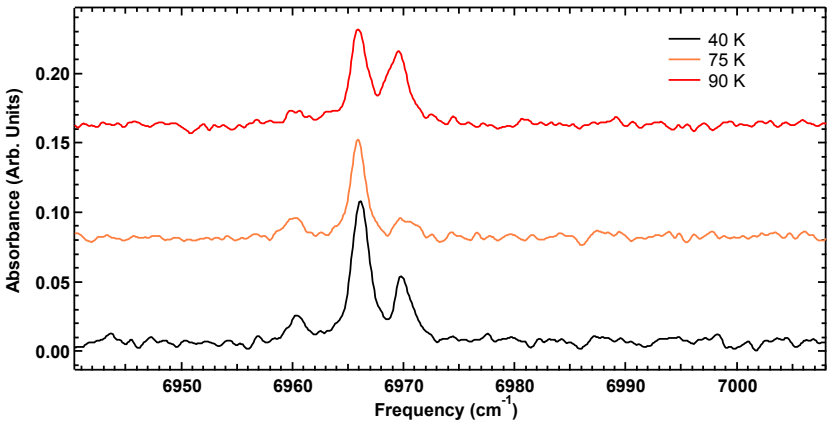

Figure 5.4: The effect of various anneal temperatures on the observed HD overtone spectra for the a concentration of 0.11 H_2/Cu. The three temperatures shown are 40 K (black), 70 K (orange), and 90 K (red). The spectra are offset for clarity.

likely possesses a higher concentration compared to that in the center. These two facts ensure that true thermal equilibrium is difficult to achieve. Since the DRIFTS optics is particularly sensitive to these surface effects, the observed IR spectra can be severely distorted, yielding peaks at low concentrations that should not be seen. Annealing the samples should in principle reduce this error, and the result of three different anneals at the same concentration is shown in Figure 5.4.

In this figure, HD overtone peaks are shown for a concentration of 0.11 H_2/Cu. Each spectrum was taken at approximately 15 K, but with different anneal temperatures of 40, 70, and 90 K. As mentioned in section 4.8, each anneal consisted of heating rapidly from base and then cooling down at a rate of 5 K/min. A significant 6969 cm^{-1} peak is apparent in the 40 K anneal spectrum. However at such a low concentration, this peak should not have the observed intensity. A longer anneal up to 70 K drastically reduces the intensity of this peak, while leaving the 9666 cm^{-1} peak relatively unchanged. The 90 K anneal, however, also gave the problematic peak at 6969 cm^{-1},

suggesting that thermal equilibration remains a complex procedure in the MOF. Because of the quality of the above 70 K anneal spectrum, most spectra presented in this thesis had an anneal temperature of 75 K.

The differences between the 40 K and 70 K anneal spectra suggest that HD molecules are unable to diffuse through the MOF even up to 40 K, and a higher anneal temperature is required to yield thermal equilibrium. In particular this calls into question the validity of the observed concentration effects seen in Peterson et al. [9] and in Callear et al. [10], for in those works, the researchers loaded D_2 at 30-55 K and 35 K respectively. This need for high-temperature anneals likely arises because of the high binding energy of HKUST-1 (see Table 5.1). Previous work in the FitzGerald lab showed that a 40 K anneal was sufficient for MOF-5, which possessed an estimated maximum binding energy of 4 kJ/mol, whereas the lowest estimate of HKUST-1 suggests a binding energy of 6 kJ/mol. Thus the molecules need more thermal energy in order to escape the MOF.

Further confirmation of the need for high anneal temperatures can be seen in Figure 5.5. To generate this figure, the sample was heated from base to 150 K at a constant rate. The external pressure was monitored, and the derivative of this pressure was plotted vs. temperature. As can be seen in the figure, there are two main regions in which gas escapes the MOF. The first region occurs from approximately 20 to 30 K, and is most likely the thermally-conductive helium gas that is needed for our experiments. The second occurs after 60 K and is the molecular hydrogen. This suggests that at temperatures below 60 K, the hydrogen does not possess sufficient thermal energy to leave the material. It is therefore reasonable to conclude that hydrogen molecules adsorbed to strong binding sites on the surface cannot escape, and consequently, thermal equilibrium at low temperatures cannot be achieved unless an anneal temperature greater than 70 K is used.

The fact the hydrogen does not leave the system in any significant man-

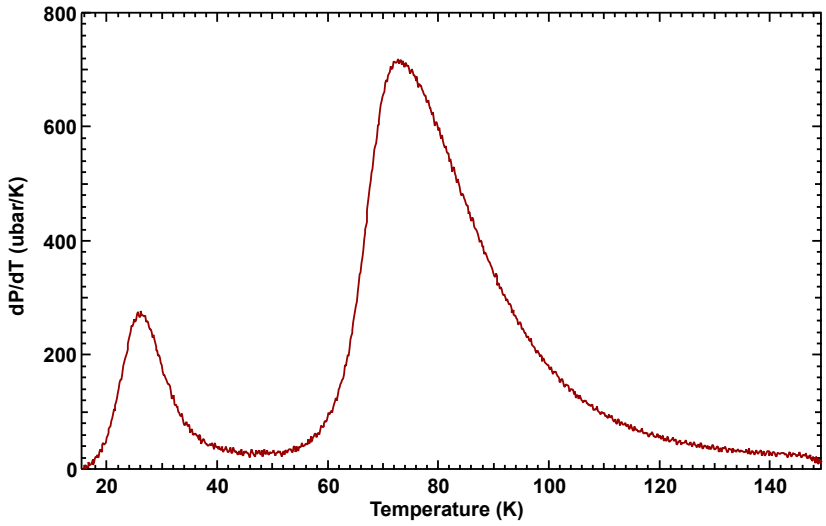

Figure 5.5: A Temperature Programmed Desorption (TPD) of H_2 in HKUST-1. Note that the initial peak at low temperatures is very likely the helium that is used as a thermal conductor in the experiment.

ner before 60 K allows us to identify the 6963 cm^{-1} peak in the HD overtone spectra. Figure 5.6 shows spectra taken sequentially at 15 (black), 20 (orange), 25 (red), 30 (light blue), 35 (dark blue), and 40 K (violet). These spectra represent roughly the same concentration of HD in the system, and so statistical mechanical arguments suggest that the fraction of molecules in the J=1 state should increase with increasing temperature while that in the ground state decreases. The peak corresponding to the J=1 state should therefore increase. This is exactly what occurs with the peak at 6963 cm^{-1}, and so we can confidently assign it to the J=1 state.

5.4 Theoretical Models

In order to test the various models, we assume that the areas of an infrared adsorption peak are directly proportional to the number of hydrogen

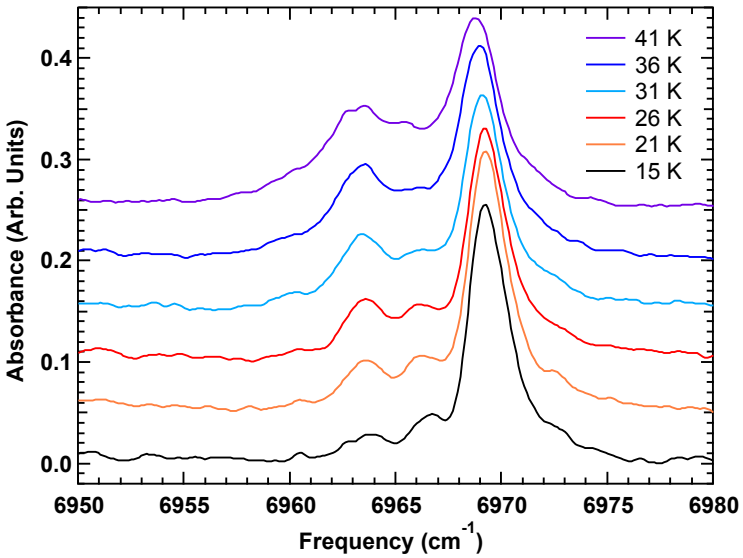

Figure 5.6: Temperature dependence of the J=1 HD overtone peak

molecules at that electronic environment. Thus any scaled plot of the areas can be compared with theoretically predicted occupancy of different sites.

5.4.1 Single and Double Occupancy

The most likely model to explain the observed 2 cm^{-1} splitting in the Q region is that the molecular hydrogen at the primary site modifies the copper paddlewheel such that the potential energy surface is different for the second hydrogen molecule that binds to that paddlewheel. We shall refer to a paddlewheel with only one hydrogen molecule as the singly-occupied state, and that with two hydrogen molecules as the doubly occupied. Pictures of these states are shown in Figure 5.7.

In this model, we assume that the peaks seen at low concentrations in both the molecular hydrogen and HD absorbance spectra are associated with the singly-occupied state, and the later peaks are with the double-occupancy.

Figure 5.7: The singly occupied state (left) and doubly occupied (right) states of the HKUST-1 primary site.The blue atoms are copper, the black are carbon, the red are oxygen, and the green are the hydrogen

As can be seen in Figure 5.8, the areas of the lower peak increase until reaching a concentration of 0.5 H_2/Cu before diminishing, whereas the area of the upper peaks grows throughout, thereby following the visual trends seen in Figure 5.3. To try and recreate the shape of these two areas, we calculated several curves with a simple statistical mechanics model that includes an energy preference for singly-occupancy vs. doubly-occupancy. These various predictions are shown in Figure 5.9 for the singly-state being energetically preferred. The predictions for having the doubly-occupied energetically preferred are shown in Figure 5.10. In these figures, the solid lines represent the calculated number of singly-occupied copper paddlewheels, and the dashed represent the double-occupancy ones. The two are color-coordinated such that the predictions for the same energy difference have the same color. Calculations were performed for energy differences of 10, 30, 50, 70, and 130 K between the singly and doubly occupied states. In the first figure, as the energetic preference for singly-occupied versus doubly-occupied is increased, the solid curve approaches a triangle, meaning that every possible paddlewheel is occupied by one hydrogen molecule before doubling occurs. By comparing

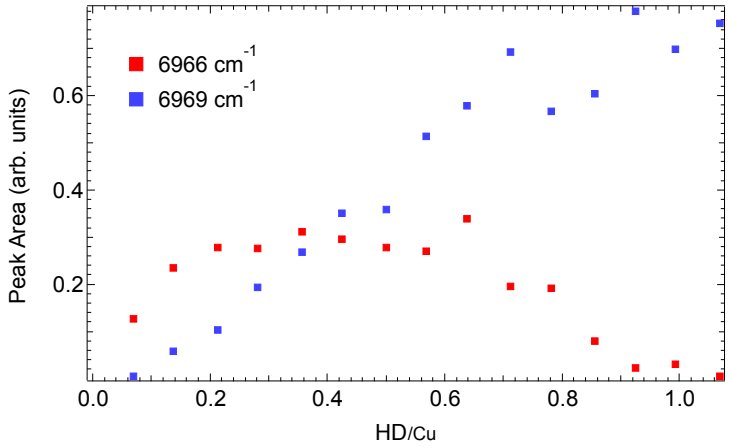

Figure 5.8: The areas of HD Overtone peaks fitted to a mixed Gaussian-Lorenztian Model verus concentration. The red points represent the areas of the 6966 cm^{-1} peak whereas the blue are the areas of the peak at 6969 cm^{-1}.

the Figures 5.8 and 5.9, it is apparent that the observed areas follow the same trend as the model, but do not agree with any energetic preference. Additionally at higher concentrations, the double-occupancy peak is systematically lower than that of the predicted. This is most likely due to limitations in the model, which inherently assumes that the paddlewheels are the only possible binding sites in the MOF. We know this is not true, and it seems reasonable that secondary sites play a more significant role as the primary saturates. This assumption is supported by the fact that the neutron diffraction data from Callear et al. demonstrated that at a loading concentration of 1 H_2/Cu, only 0.75 H_2/Cu was bound to the primary site (See Figure 8.1 in the appendix). This fact however should be taken cautiously due to the temperature effects mentioned earlier. In Figure 5.10, the single-occupancy concentration gets rapidly compressed as the energy difference is increased, so the double occupancy concentration approaches a straight line. By comparing this figure with the experimental data included in Figure 5.8, it can

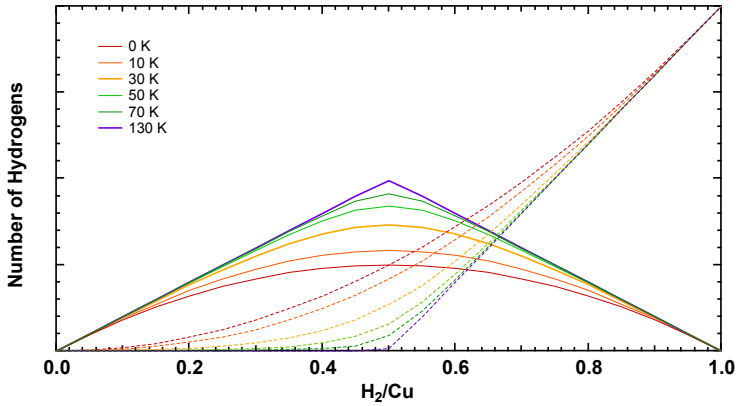

Figure 5.9: The proportion of singly-occupied to doubly-occupied paddlewheels for various energetic preferences for the singly-occupied state. The solid lines represent the singly-occupied fraction, and the dashed represent the doubly-occupied. The various energetic preferences are 0 K (red),10 K (dark orange), 30 K (light orange), 50 K (light green), 70 K (dark green), and 130 K (purple).

be immediately seen that the two do not agree for large differences. Thus if an energetic preference exists, it must be for the singly-occupied state.

5.4.2 Nearest-Neighbor Model

An alternative explanation for the observed trends is to assume it results from hydrogen-hydrogen interactions from neighboring paddlewheels. The hydrogen within a particular large pore forms a cuboctahedron, as shown in Figure 5.12, where each individual hydrogen can have up to four other H_2 molecules as nearest neighbors at a distance of 5.644 Å. In this geometry, each HD molecule corresponds to a vertex on the polygon, and the four nearest neighbors are the vertices that create triangles with this original vertex.

Using a simple model that assumes completely random binding to the paddlewheels, the relative numbers of HD with 0, 1, 2, 3, and 4 nearest neighbors are plotted versus the total HD/Cu concentration in Figure 5.13.

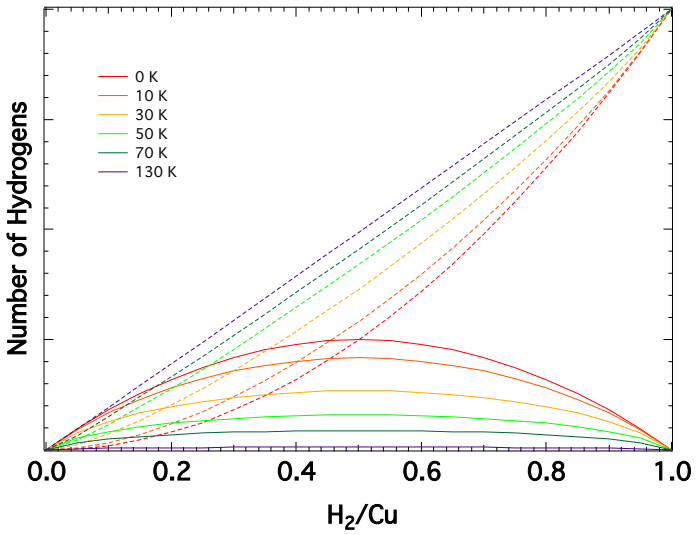

Figure 5.10: The proportion of singly-occupied to doubly-occupied paddlewheels for various energetic preferences for the singly-occupied state. The solid lines represent the singly-occupied fraction, and the dashed represent the doubly-occupied. The various energetic preferences are 0 K (red), 10 K (orange), 30 K (gold), 50 K (light green), 70 K (dark green), and 130 K (purple).

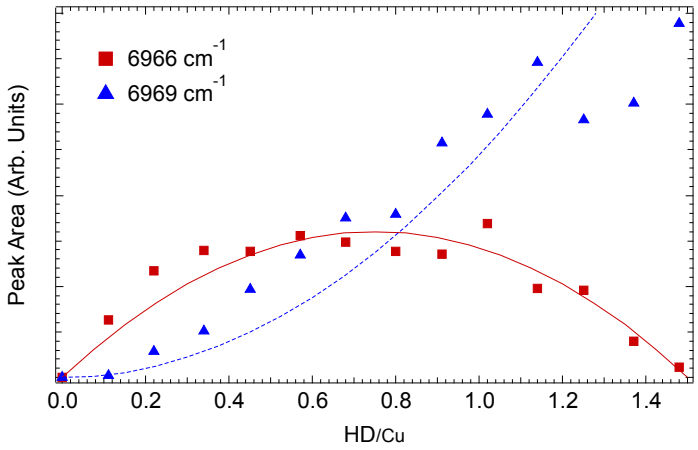

Figure 5.11: The relative proportion of singly-occupied to doubly-occupied paddlewheels for various energetic preferences for the singly-occupied state. Solid lines represent the singly-occupied fraction, and the dashed represent the doubly-occupied. The energetic preference is for 0 K.

Now if unique peaks arose for each possible number of neighbors, one would expect to be able to see 4 peaks in the middle regime. However, if the peaks are convoluted in a particular manner, then two peaks could result from the various sums of hydrogens with different numbers of neighbors. These different sums, as well as the scaled experimental HD peak areas from Figure 5.8 areas are shown in Figure 5.14. Notice that the experimental areas do not appear to lie well along any of the predicted curves. Additionally, as mentioned in section 5.1, a uniform splitting between ortho and para hydrogen suggests negligible anisotropic interactions. Thus, only isotropic interactions are possible, and these do not create a significant enough energy splitting unless the hydrogen is extremely modified [36].

A preliminary estimate of the effect of the hydrogen modification would be to assume that the MOF induces a permanent dipole. This dipole most likely cannot be bigger than that of normal molecular dipoles such as nitric

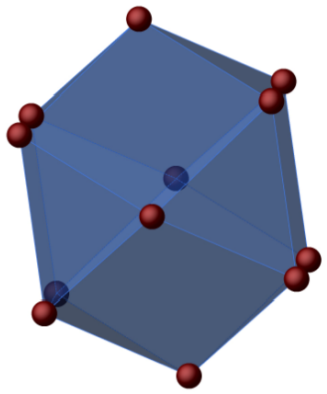

Figure 5.12: The cuboctahedron formed by the 12 hydrogen molecules bound to the primary site. Each molecule is a vertex, with four nearest neighbors at a distance of 5.6 Å. These neighbors are the other vertices that form the equilateral triangles.

oxide (NO). We shall therefore use 0.33 Debye in our calculation, which is twice the dipole value for NO. This will act as a maximum possible dipole moment for this effect. The energy W related to the interaction of two dipoles $\boldsymbol{\mu_1}$ and $\boldsymbol{\mu_2}$ is:

$$W = \frac{1}{4\pi\epsilon_0}\left(\frac{\boldsymbol{\mu_1}\cdot\boldsymbol{\mu_2}}{r^3} - \frac{3(\boldsymbol{\mu_1}\cdot\boldsymbol{r})(\boldsymbol{\mu_2}\cdot\boldsymbol{r})}{r^5}\right), \tag{5.1}$$

where $\boldsymbol{r}$ is the separation vector [11]. For a preliminary interpretation, it is acceptable to assume that the two dipoles are parallel to each other and parallel to the separation vector. This yields an interaction energy of 6 cm^{-1} (8.4 K) at the 5.6 Å distance (see section 3.3). Thus the 10 % rule (see Section 2.5) suggests the interaction of one dipole with a single nearest neighbor dipole is too small to cause the observed splitting. Additionally, since this dipole cannot possibly align with all of its nearest neighbors, the interactions from all of the possible nearest neighbors will most likely average, suggesting that the above interaction truly estimates the maximum possible interaction

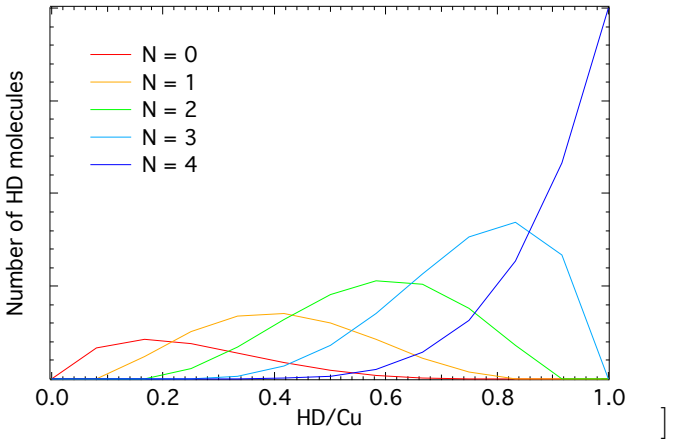

Figure 5.13: The number of HD molecules with 0 (red),1 (yellow),2 (green),3 (light blue), or 4 (dark blue) nearest neighbors as a function of concentration. In this calculation the total number of HD molecules is 2000.

energy. Induced dipoles on the hydrogen molecules from HKUST-1 therefore do not appear to be the source of the observed splitting.

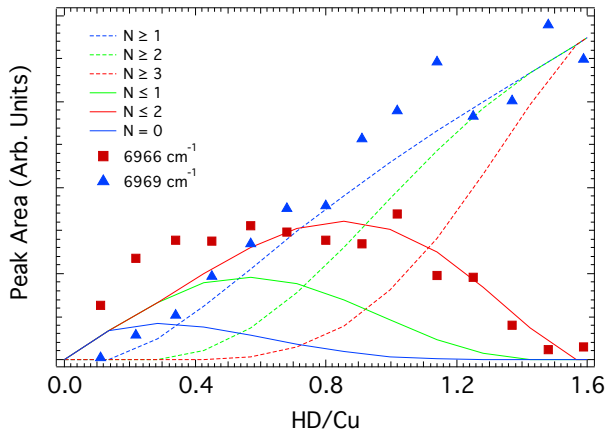

Figure 5.14: Expected numbers of HD molecules with various numbers of nearest neighbor hydrogens as functions of concentration. The red curves represent the HD molecules with 2 or less nearest neighbors or more than 3. The green curves are for hydrogens with one or zero neighbors, or 2 or more. The blue represent those with no neighbors or 1 or more. The black triangles and squares are scaled version of the HD overtone areas shown in Figure 5.8. Note that this model assumes no preference for filling.

Chapter 6

Future Work

6.1 High-Resolution Spectrum of the HD Overtones

In addition to the previously shown spectra, we also obtained an HD overtone spectrum with a high signal-to-noise ratio. This spectrum is shown below in Figure 6.1. The peaks at the leftmost part of this graph are the ordinary HD overtones discussed earlier in section 5.2, while the other smaller peaks are new ones only observed with low background noise. The frequencies of these smaller peaks as well as the difference between those frequencies and the double-occupancy HD peak (6969 cm^{-1}) are shown in Table 6.1.

These peaks have not yet been identified, and were only visible by averaging over an unusually large number of scans. However if we assume a simple-harmonic potential such that the frequency shifts scale as $\frac{1}{\mu}$, then the inelastic neutron scattering from Callear et al. predicts the energy separation between the ground and 1st excited translational state to be on the order of 80 cm^{-1}, and the excitation from the translational ground to the first overtone to be on the order of 130 cm^{-1}. We can therefore tentatively suggest

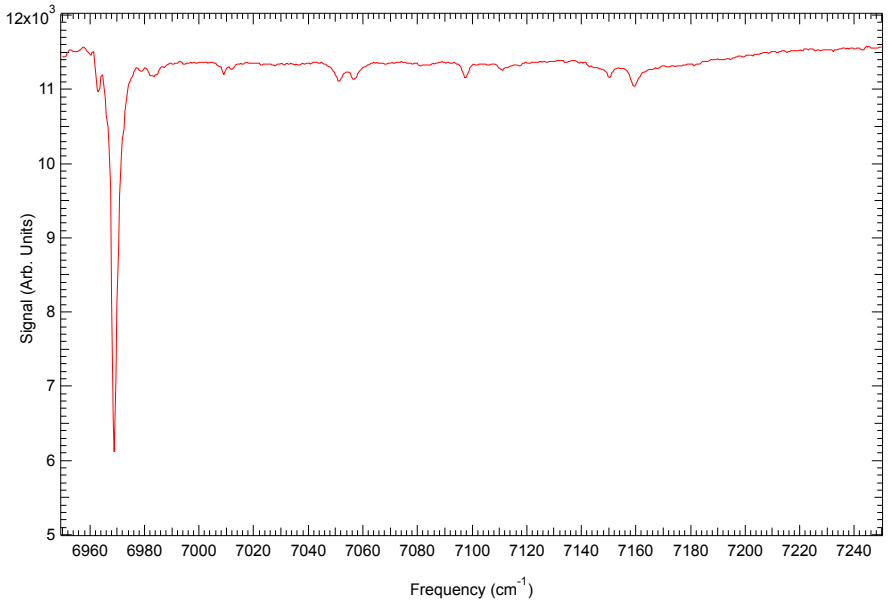

Figure 6.1: HD Overtones Nice

that the peaks at 7051, 7097, and 7011 cm^{-1} could be excitations to the first and second excited translational states. If the peaks are truly the result of vibrational overtones and translations, this is the first known observation of these peaks [29]. In the future we hope to obtain more high resolution spectras of the HD overtone region and test whether these peaks are translations. However, the other peaks listed in Table 6.1 remain unexplained.

6.2 Other MOFS with the Copper Paddlewheel Structure

As shown earlier, we propose two possible models to explain the observed splitting in HKUST-1. The nearest-neighbor model, however, is very sensitive to the distance between the copper paddlewheels. Thus studying a series of MOFs with copper paddlewheels and various unit cell sizes such as the

Table 6.1: The frequencies of the small HD overtone peaks as well as their difference from the fundamental HD overtone peak.

Frequency (cm^{-1})	Frequency Shift (cm^{-1})
6983	14
7009	40
7012	43
7051	82
7057	88
7097	128
7111	142
7150	181
7159	190

NOTT-100 series could help to discern the validity of either theory.

Chapter 7

Conclusion

In conclusion, we have examined the interaction of the Metal Organic Framework HKUST-1 with molecular hydrogen and its isotopes at cryogenic temperatures using infrared spectroscopy. We have seen a 2 cm^{-1} splitting of the $Q_1(0)$ and $Q_1(1)$ peaks as well as a corresponding 3 cm^{-1} peak in the HD overtone spectrum. As far as we are aware, this is the first time that such a splitting has been observed. We have proposed two possible mechanisms to explain this splitting, of which we suspect the single and double occupancy model to be the most likely. Difficulties in measuring peak intensities, however, prevented good agreement with the theoretical model.

Chapter 8

Appendix

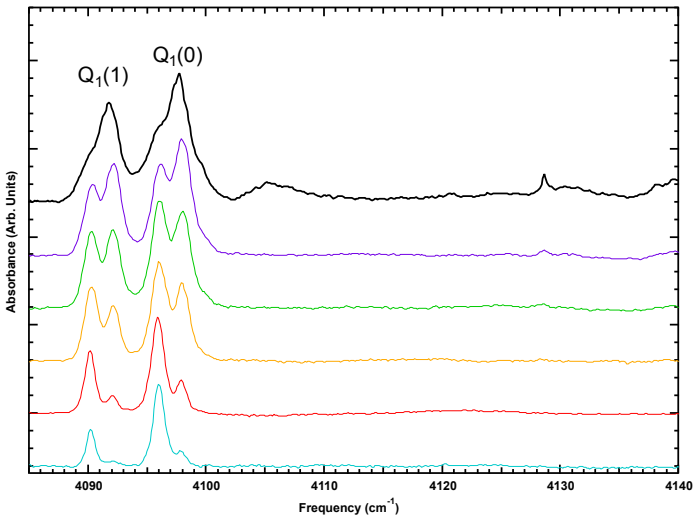

Figure 8.1: Adsorption spectra for HKUST-1 Q region including secondary sites. The concentrations shown are 0.1 (blue), 0.22 (red), 0.45 (orange), 0.7 (green), 0.9 (purple), and 1.37 (black) H_2/Cu.

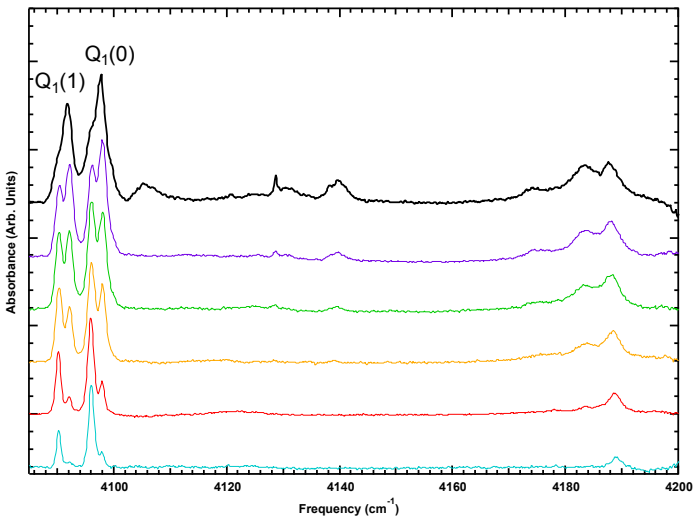

Figure 8.2: Adsorption spectra for HKUST-1 Q region including translational peaks.The concentrations shown are 0.1 (blue), 0.22 (red), 0.45 (orange), 0.7 (green), 0.9 (purple), and 1.37 (black) H_2/Cu.

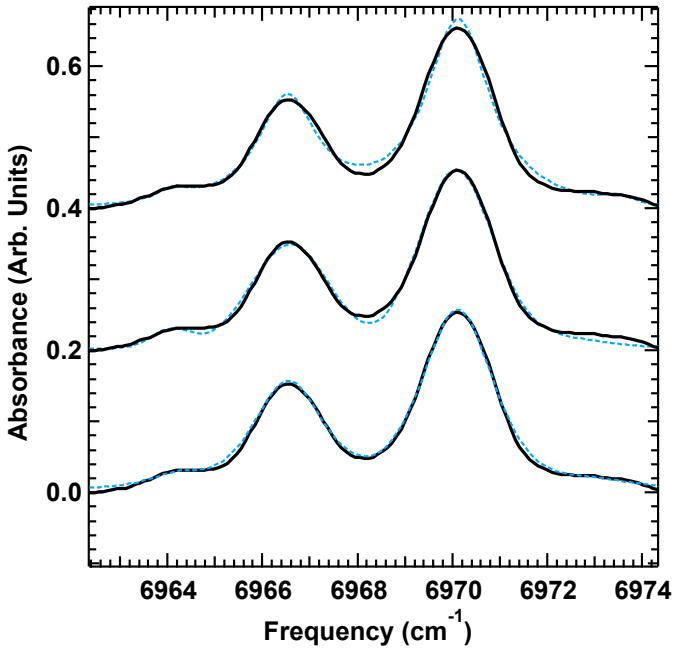

Figure 8.3: The 3 types of peak models used to fit the experimental data. The black curves are all the same experimental file, and the dashed are the different fits. The lowest of the three fits is the mixed gaussian and lorentzian, the middle is the pure gaussian fit, and the top is the pure lorenztian.

Bibliography

[1] Stephen F. Lincoln. Fossil fuels in the 21st century. *Ambio*, 14:621–627.

[2] M. P. Suh, H. J. Park, T. K. Prasad, and D. Lim. Hydrogen storage in metal-organic frameworks. *Chemical Review*, 112:782–835, 2012.

[3] Department of Energy Hydrogen and Fuel Cells Program Plan. An integrated strategic plan for the research, development, and demonstration of hydrogen and fuel cell technologies, 2011.

[4] Suresh K. Bhatia and Alan L. Myers. Optimum conditions for adsorptive storage. *Langmuir*, 22:1688–1700, 2006.

[5] Ehud Tsivion, Jeffrey R. Long, and Martin Head-Gordon. Hydrogen physisorption on metal-organic framework linkers and metalated linkers: A computational study of the factors that control binding strength. *Journal of the American Chemical Society*, 136:17827–17835, 2014.

[6] Leslie J. Murray, Mircea Dincă, and Jeffrey R. Long. Hydrogen storage in metal-organic frameworks. *Chemical Society Reviews*, 38:1294–1314, 2009.

[7] Hong-Cai Zhou, Jeffrey R. Long, and Omar M. Yaghi. Introduction to metal-organic frameworks. *Chemical Reviews*, 112:673–674, 2012.

[8] Rachel B. Getman, Youn-Sang Bae, Christopher E. Wilmer, and Randall Q. Snurr. Review and analysis of molecular simulations of methane, hydrogen, and acetylene storage in metal-organic frameworks. *Chemical Reviews*, 112:703–723, 2012.

[9] Vanessa K. Peterson, Craig M. Brown, Yun Liu, and Cameron J. Kepert. Structural study of d_2 within the trimodal pore system of a metal organic framework.

[10] Samantha K. callear, Anibal J. Ramierz-Cuesta, William I. David, Franck Millange, and Richard I. Walton. High-resolution inelastic neutron scattering and neutron powder diffraction study of the adsorption of dihydrogen by the cu(ii) metal-organic framework material hkust-1. *Chemical Physics*, 427:9–17, 2013.

[11] David J. Griffiths. *Introduction to Electrodyanmics*. Pearson, 4 edition, 2013.

[12] M. Trefler and H.P. Gush. Electric dipole moment of hd. *Physical Review Letters*, 20:703–705, 1968.

[13] David. J. Griffiths. *Introduction to Quantum Mechanics*. Pearson, Upper Saddle River, NJ, 2 edition, 2005.

[14] W. Kolos and L. Wolniewicz. Polarizability of the hydrogen molecule. *Journal of Chemical Physics*, 46:1426–1432, 1966.

[15] Jesse B. Hopkins. Honor's thesis:infrared spectroscopy of h_2 trapped in metal organic frameworks, 2009.

[16] Stephen A. FitzGerald, Jocienne Nelson, Elizabeth Gilmour, and Jesse L.C. Rowsell. Infrared overtone spectroscopy of adsorbed hydrogen in mof-5. *Journal of Molecular Spectroscopy*, 307:20–26, 2015.

[17] Hugh Churchill. Honor's thesis:low-temperature infrared spectroscopy of h_2 in solid c_{60}, 2006.

[18] B. P. Stoicheff. High resoltuion raman spectroscopy of gasses, ix. spectra of h_2, hd, and d_2. *Canadian Journal of Physics*, 35:730–741, 1957.

[19] Gerhard Herzberg. *Molecular Spectra and Molecular Structure, I. Diatomic Molecules*. Prentice-Hall, Inc., New York, 1939.

[20] Philip M. Morse. Diatomic molecules according to the wave mechanics. ii. vibrational levels. *Physical Review*, 34:57–64, 1929.

[21] H. Hamaguchi, I. Suzuki, and A.D. Buckingham. Determination of derivatives of the polarizability anisotropy anisotropy in diatomic-molecules.1. theoretical considerations on vibration-rotation raman intensities. *Mol. Phys.*

[22] Stephen S.-Y. Chui, Samuel M.-F. Lo, Jonathan P.H. Charmant, A. Guy Orpen, and Ian D. Williams. A chemically functionalizable nanoporous material $[cu_3(tma)_2(h_2o)_3]_n$. *Science*, 283:1148–1150, 1999.

[23] Craig M. Brown, Yun Liu, Raner Yildirim, Vanessa K Peterson, and Cameron J Kepert. Hydrogen adsorption in hkust-1: A combined inelastic neutron scattering and first-principles study. *Nanotechnology*, 20:1–11, 2009.

[24] Jesse L. C. Rowsell and Omar M. Yaghi. Effects of functionalization, catenation, and variation of the metal oxide and organic linking units on the low-pressure hydrogen adsorption properties of metal-organic frameworks. *J. Am. Chem. Soc.*, 128:1304–1315, 2006.

[25] Jenny G. Vitillo, Laura Regli, Sachin Chavan, Gabriele Ricchiardi, Giuseppe Spoto, Pascal D. C. Dietzel, Silvia Bordiga, and Adriano

Zecchina. Role of exposed metal sites in hydrogen storage in mofs. *J. Am. Chem. Soc.*, 130:8386–8396, 2008.

[26] Y. Liu, C.M. Brown, D.A Neumann, V.K. Peterson, and C.J. Kepert. Inelastic neutron scattering of h_2 adsorbed in hkust-1. *Journal of Alloys and Compounds*.

[27] S. Bordiga, L. Regli, F. Bonino, E. Groppo, C. Lamberti, B. Xiao, P.S. Wheatley, R.E. Morris, and A. Zecchina. Adsoprtion properties of hkust-1 toward hydrogen and other small molecules monitored by ir. *Phys. Chem. Chem. Phys.*, 9:2676–2685, 2007.

[28] S.A. FitzGerald, H.O.H. Churchill, P.M. Korngut, C.B. Simmons, and Y.E. Strangas. Cryogenic apparatus for diffuse reflectance infrared spectroscopy with high-pressure capabilities. *Rev. Sci. Instrum.*, 77, 2006.

[29] Jocienne Nelson. Honor's thesis: Overtone spectroscopy of hydrogen in mof-5, 2014.

[30] B.P. Stoicheff. High resolution raman spectroscopy of gasses, ix. spectra of h_2, hd, and d_2. *Canadian Journal of Physics*, 35:730–741, 1957.

[31] H. Hamaguchi, I. Suzuki, and A. D. Buckingham. Determination of derivatives of the polarizability anisotropy in diatomic-molecules.1. theoretical considerations on vibration-rotation raman intensities. 43:963–973, 1981.

[32] S.L. Bragg, J. W. Brault, and W. H. Smith. Line positions and strengths in the h_2 quadrupole spectrum. *The Astrophysical Journal*, 263:999–1004, 1982.

[33] S. Kassi and A. Campargue. Electric quadrupole and dipole transitions of the first overtone band of hd by crds between 1.45 and 1.33 μm. *Journal of Molecular Spectroscopy*, pages 36–42, 2011.

[34] S. Kassi, A. Campargue, K. Pachucki, and J. Komasa. The absorption spectrum of d_2: Ultrasensitive cavity ring down spectroscopy of the (2-0) band near 1.7 μm and accurate ab initio line list up to 24000 cm^{-1}. *J. Chem. Phys.*, 136, 2012.

[35] Stephen A. FitzGerald, Christropher T. Eckdahl, Cooper S. McDonald, Jocienne N. Nelson, Kai Shinbrough, Holden W.H. Lai, and Jesse L.C. Rowsell. Orientational ortho-h_2 pair interactions in the microporous framework mof-5. *Phys. Rev. B*, 92, 2015.

[36] Isaac F. Silvera. The solid molecular hydrogens in the condensed phase: Fundamentals and static properties. *Rev. Mod. Phys.*, 52:393– 452, 1980.

[37] S.A. FitzGerald, K. Allen, P. Landerman, J. Hopkins, J. Matters, R. Myers, and J. L. C. Rowsell. Dynamics of adsorbed h_2 in the microporous framework mof-5 analyzed using diffuse reflectance infrared spectroscopy. *Physical Review B*, 77, 2008.

[38] Brian S. Burkholder. Honor's thesis:catalysis of conversion between the spin isomers of h_2 by mof-74, 2009.

[39] A.D. Buckingham. Solvent effects in vibrational spectroscopy. *The Faraday Society and Contributors*, pages 753–760, 1960.